OVERDAMPED DETERMINISTIC RATCHETS DRIVEN BY MULTIFREQUENCY FORCES*

David Cubero, Jesús Casado-Pascual, Azucena Alvarez
Manuel Morillo

Universidad de Sevilla, Facultad de Física
Apdo. Correos 1065, Sevilla 41080, Spain

Peter Hänggi

Institut für Physik, Universität Augsburg
Universitätsstraße 1, 86135 Augsburg, Germany

(Received February 21, 2006)

We investigate a dissipative, deterministic ratchet model in the overdamped regime driven by a *rectangular force*. Extensive numerical calculations are presented in a diagram depicting the drift velocity as a function of a wide range of the driving parameter values. We also present some theoretical considerations which explain some features of the mentioned diagram. In particular, we proof the existence of regions in the driving parameter space with bounded particle motion possessing zero current. Moreover, we present an explicit analytical expression for the drift velocity in the adiabatic limit.

PACS numbers: 05.60.–k, 05.45.Pq, 05.45.Ac, 05.45.Xt

1. Introduction and model set-up

Directed current in ratchet systems have received much attention over recent years [1–5]. One of the reasons to study these type of systems is motivated by the attempt to understand the physical mechanism of motion of molecular motors in biological systems [2,6] and to investigate its role in the design of new material properties [3, 4]. The dynamics of a particle moving in a periodic potential under the action of an applied time periodic term is rather complex and rich, displaying typically even chaotic behavior [7–10]. A feature of particular interest is the emergence of directed currents in the

* Presented at the XVIII Marian Smoluchowski Symposium on Statistical Physics, Zakopane, Poland, September 3–6, 2005.

system response to an external time-periodic driving with zero time-averaged value. Though most of the works about ratchet systems consider the presence of noise, this phenomenon may also arise in deterministic systems, both in the overdamped [11–13] and underdamped [7, 8] regimes. Moreover, the phenomenon of anticipated synchronization occurring in inertial deterministic ratchets have been studied recently [14].

In particular, in the overdamped regime, the one-dimensional particle dynamics $x(t)$ usually considered is governed by a first order differential equation of the type

$$\dot{x}(t) = -U'[x(t)] + F(t)\,, \tag{1}$$

where the dot and the prime denote time and spatial derivatives, respectively, $U(x)$ is a periodic potential with spatial period λ [*i.e.*, $U(x+\lambda)=U(x)$], and $F(t)$ is a time-periodic driving force with period T [*i.e.*, $F(t+T)=F(t)$]. In this type of systems, the current is defined as the average velocity

$$v = \lim_{t\to\infty} \frac{x(t)-x(0)}{t}\,. \tag{2}$$

As shown in Ref. [11] co-existing attractors can exist for large driving strengths, which, however, are not current-carrying. A finite current v, possessing an unbounded $x(t)$-trajectory, is consequently independent of the initial condition $x(0)$. It can also be shown that a directed current ($v \neq 0$) is only possible if at least one of the following symmetries is broken [2, 4, 5, 15]:

$$\exists x_0 \in \Re \quad \text{such that} \quad U(x_0 - x) = U(x_0 + x)\,, \qquad \forall x \in \Re\,, \tag{3}$$

$$F(t + T/2) = -F(t)\,, \qquad \forall t \in \Re\,. \tag{4}$$

Our main interest in this paper is to gain a deeper insight into these type of systems exploring some quantitative and qualitative aspects of its very rich dynamics. Specifically, we will consider the same sawtooth potential as in Refs. [11, 16]

$$U(x) = -\frac{1}{2\pi}\left[\sin(2\pi x) + \frac{1}{4}\sin(4\pi x)\right], \tag{5}$$

which has a spatial period $\lambda = 1$. In addition, rather than using a sinusoidal driving force $F(t)$, in this work we will consider a multifrequency time-periodic force given by

$$F(t) = \begin{cases} A & \text{for} \quad 0 \le t < \frac{T}{2} \\ -A & \text{for} \quad \frac{T}{2} \le t < T, \end{cases} \tag{6}$$

with A being a constant. Since the potential (5) breaks the spatial symmetry (3), a directed current is possible, even though the time symmetry (4) is fulfilled.

The paper is organized as follows. In Sec. 2, we perform a detailed numerical study of Eq. (1) for a wide range of the driving parameter values A and $\omega = 2\pi/T$. In particular, we present a colored phase-diagram v *versus* A and ω, which is inspired by the figure provided by Prof. Peter Talkner and collaborators in [16]. In order to explain some features of this diagram we propose in Sec. 3 some simple theoretical considerations. Finally, in the last section, we summarize our findings.

2. Dynamical regimes and numerical evaluation of the current

Regardless of the value of the driving frequency, there exist two critical amplitudes $A_1^* = 3/4$ and $A_2^* = 3/2$ separating three different regimes. For amplitudes $A \in [0, A_1^*]$, both potential states, $U(x) + Ax$ and $U(x) - Ax$, possess a periodic array of equilibrium points (see Fig. 1). Since the inertial term $m\ddot{x}(t)$ is absent, the particle cannot cross these equilibrium points, and consequently, it remains trapped between them, leading to a zero current. For $A \in (A_1^*, A_2^*]$, the potential state $U(x) + Ax$ retains its equilibrium points, while $U(x) - Ax$ does not have any, that allowing non-bounding motion in the positive direction. Finally, when $A > A_2^*$, neither of the potential states possesses equilibrium points, and the particle motion is not bounded in either direction.

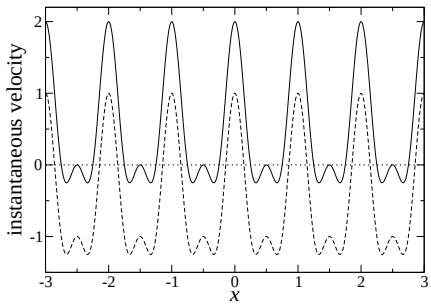

Fig. 1. Plots of the instantaneous velocities $-U'(x)+A$ (solid line) and $-U'(x)-A$ (dashed line) as a function of x for a driving force with $A = 0.5$. (All quantities in dimensionless units.)

In order to go further in our analysis, we have resorted to a numerical treatment of our model using the freely available integrator RKSUITE [17]. Wide regions of parameter space have been explored. In Fig. 2 we have used a color code to represent the drift velocity v for a rectangular driving force of varying amplitude A and frequency ω. The regions in black correspond to bounded, time-periodic particle motion with zero current. More precisely, the velocity in those regions is smaller than 10^{-6}. The diagram has a rich and interesting structure. Regions of zero drift velocity are intermingled with regions with finite values, giving rise to a finger-shaped structure.

Notice that for the parameter values considered, the drift velocity is always positive or zero, showing the largest magnitude in the intermediate region $A \in (A_1^*, A_2^*]$. This last feature could be understood by taking into account that in this regime the motion in the positive direction is never compensated by motion in the opposite direction.

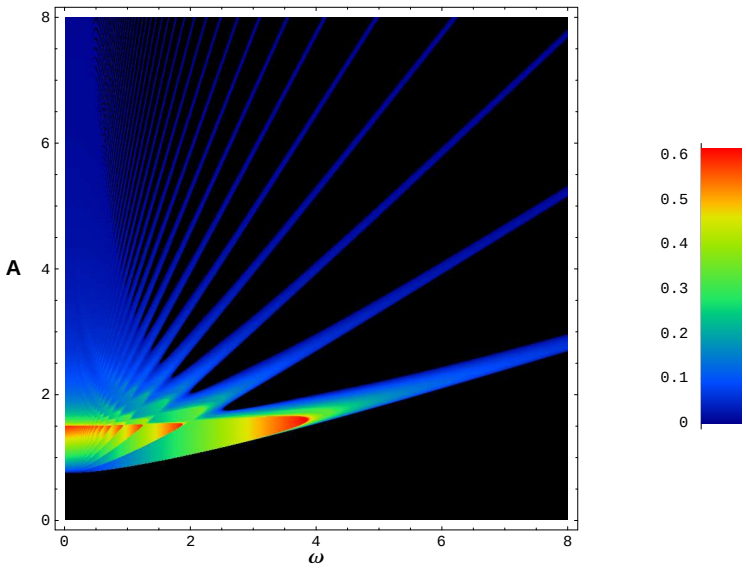

Fig. 2. The "Talkner"-current phase diagram. The drift velocity as a function of the driving parameters A and ω is represented using a color density plot. Black color has been used for velocities less than 10^{-6}. (All quantities in dimensionless units.)

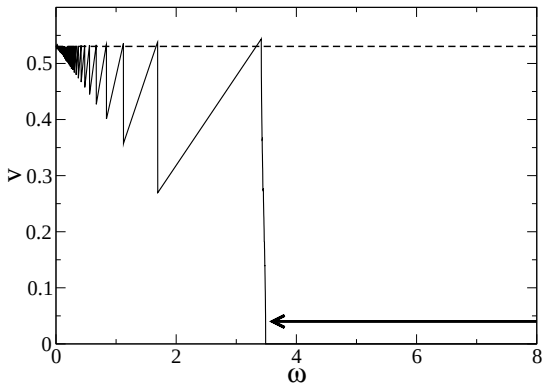

Fig. 3. Drift velocity v (solid line) as a function of the driving frequency ω for $A = 1.4 < A_2^*$. The dashed line shows the adiabatic value. The arrows depicts the zero-velocity bands given by the theory in the text. (All quantities in dimensionless units.)

In Fig. 3 we present a section of the diagram for a driving amplitude in the intermediate regime $A = 1.4$. A series of peaks corresponding to the fingers in Fig. 2 are observed. Fig. 4 shows a representative section for $A > A_2^*$. By contrast with Fig. 3, it presents an intermediate gap of particle localization. If we further increase the value of A, more intermediate gaps appear, as can be seen in the phase diagram.

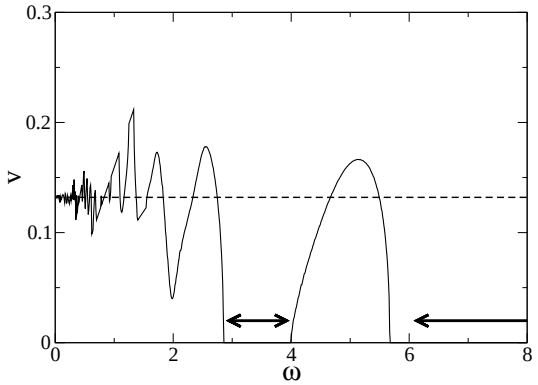

Fig. 4. The same as in Fig. 3 but for $A = 2 > A_2^*$.

3. Some theoretical results

Even though the nonlinearity of the system precludes a complete and detailed analytical solution of the problem, it is possible to explain some features of the phase diagram by simple considerations.

3.1. Proof of existence of regions displaying particle localization

Due to the truncation implicit in any numerical calculation, the simulations reported above are not able to distinguish between a situation of exact particle localization or a very small drift, lower than the tolerance we chose to determine the black regions in Fig. 2. Furthermore, a simple explanation of the existence of such regions in the non-trivial regime $A > A_1^*$ would be desirable.

Let us assume that the particle starts at x_0 at the beginning of a driving period. It then moves under a force $-U'(x) + A$ for half a period until it reaches the position $x_1 > x_0$. Then the driving force switches sign so the total force on the particle is now $-U'(x) - A$, which makes it (in general) move backwards up to a position x_0' after another $T/2$. If $x_0' = x_0$, the particle has returned to the initial position, and consequently, the process is repeated successively, leading to a drift velocity strictly equal to zero. For this situation to happen the following equations must hold

$$\frac{T}{2} = \int_{x_0}^{x_1} \frac{dx}{-U'(x) + A} \tag{7}$$

$$\frac{T}{2} = \int_{x_1}^{x_0} \frac{dx}{-U'(x) - A} \,. \tag{8}$$

Subtracting both equations we arrive at the condition

$$G(x_0) = G(x_1) \,, \tag{9}$$

where

$$G(x) = \int_0^x d\tilde{x} \frac{U'(\tilde{x})}{A^2 - U'(\tilde{x})^2} \,. \tag{10}$$

Therefore, we can determine the set of pairs (x_0, x_1) with zero current for a given driving strength A by plotting the function $G(x)$ *versus* x (see Fig 5). The intersection of a horizontal line with $G(x)$ in this plot provides the possible values of the pair (x_0, x_1). The period T associated with the pair is then given by Eq. (7) or (8). Since the drift velocity v is independent of the initial conditions [15], it would be exactly zero for those driving parameter values A and T.

In Fig. 5, we plot $G(x)$ for the same value of $A = 2 (> A_2^*)$ as in Fig. 4. A horizontal line crosses $G(x)$ at the points A, B, C, and D, providing the

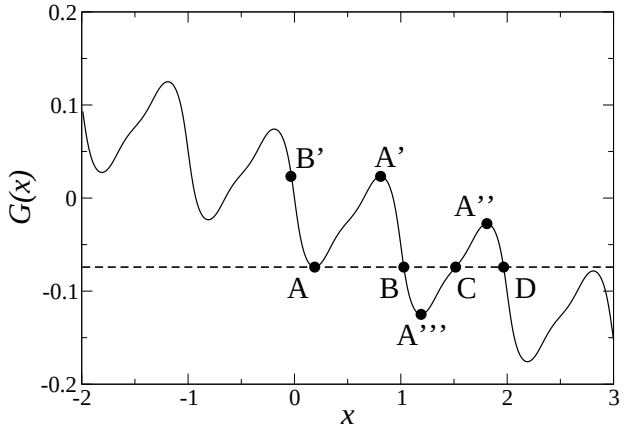

Fig. 5. Determination of zero-velocity bands with $x(t+T) = x(t)$. Solid line depicts $G(x)$, defined in Eq. (10), as a function of x for the same value of A as in Fig. 4.

coordinates $x_{\rm A}, x_{\rm B}, x_{\rm C}$, and $x_{\rm D}$. If we choose $x_0 = x_{\rm A}$, and x_1 as any of the other points, we obtain three pairs of points with driving periods $T_{\rm AB}, T_{\rm AC}$, and $T_{\rm AD}$. Since the integrand in Eq. (7) is always positive, the further away x_1 is from x_0, the larger the period, which implies $T_{\rm AB} < T_{\rm AC} < T_{\rm AD}$.

Before we proceed in analyzing the plot in greater detail, let us study the symmetries of $G(x)$. Since it is an integral of a space-periodic function [see Eq. (10)] we have

$$G(x+1) = G(x) + \phi\,, \tag{11}$$

where $\phi = G(1)$. In addition, taking into account that $U'(x)$ is an even function, necessarily

$$G(-x) = -G(x)\,. \tag{12}$$

Property (11) leads to the fact that we only need to vary x_0 within a spatial interval of length unity, whereas property (11) combined with (12) implies that $G(x)$ has an inversion center at $x = n$, with n any integer. The driving period T, when viewed as a function of x_1 or x_0 [see Eq. (7)], also obeys these properties.

Because of these symmetry properties, choosing the point A as x_0 in Fig. 5 is equivalent to choosing any of the points A$'$, A$''$ and A$'''$, in the sense that they lead to the same driving periods. Let us consider a horizontal line between points A and A$'$. As this line gets closer to A, two of the intersection points approach each other, and consequently, the driving period associated to them tends to zero. Therefore, $T = 0$ ($\omega = \infty$) corresponds to particle localization. Moving up the line continuously we obtain a whole band of driving periods starting from zero up to a maximum value given by the pair $(x_{\rm B'}, x_{\rm A'})$ when the line crosses A$'$. This pair is equivalent to $(x_{\rm A}, x_{\rm B})$. Two more intermediate periods in the band can be obtained from the pairs $(x_{\rm B}, x_{\rm C})$ and $(x_{\rm C}, x_{\rm D})$ in the figure.

The next value of the driving period obtained from Fig. 5 is the one given by the pair $(x_{\rm A}, x_{\rm C})$. This pair marks the start of a second band that ends at the maximum value given by the pair $(x_{\rm A}, x_{\rm D})$. Moving up the line up to A$''$ gives all the intermediate values in the band.

Clearly, the first band is associated with movement within a spatial interval less than unity (*i.e.*, $0 \leq x_1 - x_0 < 1$), whereas the second band is related to displacements two times that distance ($1 \leq x_1 - x_0 < 2$). In Fig. 4 we have indicated with arrows the calculated frequency bands. It can be seen that they do not cover the entire region with numerically evaluated zero velocity. This is due to the fact that the above discussed mechanism is just the simplest one leading to zero current. The drift velocity can also vanish because the particle returns to its initial position after two or more driving periods, instead of after the first one.

The same analysis can be carried out for a subthreshold driving $A \in (A_1^*, A_2^*]$. In this case $G(x)$ presents singularities at the equilibrium points, which prevents the particle from crossing those points when $F(t) = -A$. This leads to a single band which is near the zero-current region observed in the simulations, as shown in Fig. 3.

3.2. Adiabatic limit

In this section we will obtain an analytical expression for the current in the adiabatic limit $\omega \to 0$

$$v_{\rm ad}(A) = \lim_{\omega \to 0} v(A, \omega)\,. \tag{13}$$

Specifically, as proved later on, $v_{\rm ad}(A)$ is given by the average value

$$v_{\rm ad}(A) = \frac{1}{2}\left[v_+(A) + v_-(A)\right]\,, \tag{14}$$

where $v_+(A)$ and $v_-(A)$ are, respectively, the velocities in the presence of the static forces $-U'(x) + A$ and $-U'(x) - A$. Obviously, $v_+(A) = 0$ for $A \in [0, A_1^*]$ and $v_-(A) = 0$ for $A \in [0, A_2^*]$, as the particle ends up being trapped by an equilibrium point. For $A > A_1^*$,

$$v_+(A) = \frac{1}{\tau_+(A)}\,, \tag{15}$$

where

$$\tau_+(A) = \int_0^1 \frac{dx}{A - U'(x)} = \frac{2\sqrt{2A + \sqrt{-3 + 4A(1+A)}}}{\sqrt{(-1+2A)(3+2A)(-3+4A)}} \tag{16}$$

is the time taken for the particle to travel a distance equal to 1 (the spatial period) in the presence of the static force $-U'(x) + A$. Analogously, for $A > A_2^*$,

$$v_-(A) = \frac{-1}{\tau_-(A)}\,, \tag{17}$$

where

$$\tau_-(A) = \int_0^1 \frac{dx}{A + U'(x)} = \frac{\sqrt{4A + 2\sqrt{3+4A}} + \sqrt{4A - 2\sqrt{3+4A}}}{\sqrt{(-3+2A)(1+2A)(3+4A)}} \tag{18}$$

is defined as $\tau_+(A)$ but replacing $-U'(x) + A$ by $-U'(x) - A$.

In order to prove Eq. (14), let us consider separately the three regimes $A \in [0, A_1^*]$, $A \in (A_1^*, A_2^*]$, and $A \in (A_2^*, \infty)$. For $A \in [0, A_1^*]$ the result in Eq. (14) is trivial, since $v_{\rm ad}(A) = v_-(A) = v_+(A) = 0$. In the intermediate regime $A \in (A_1^*, A_2^*]$, let us assume that the particle is initially located at a minimum of the potential $U(x) + Ax$ (as we have mentioned before, the drift velocity does not depend on this particular initial condition). If we choose the time period of $F(t)$ as $T = 2N\tau_+(A)$, with $N = 1, 2, 3, \ldots$, then, during the first half-period, $N\tau_+(A)$, the particle stays trapped at the initial location. After the second half-period, $2N\tau_+(A)$, the particle arrives at a new minimum of $U(x)+Ax$ separated from the initial location by a distance N. During the third half-period, $3N\tau_+(A)$, the particle stays trapped at that minimum, and so on. Thus, for a given $A \in (A_1^*, A_2^*]$, all the frequencies

$$\omega_N(A) = \frac{\pi}{N\tau_+(A)} \tag{19}$$

lead to the same value of the drift velocity

$$v\left[A, \omega_N(A)\right] = \frac{N}{2N\tau_+(A)} = \frac{1}{2\tau_+(A)} = \frac{v_+(A)}{2}\,. \tag{20}$$

Consequently, taking into account that $\lim_{N\to\infty} \omega_N(A) = 0$, it follows that

$$v_{\rm ad}(A) = \lim_{N\to\infty} v\left[A, \omega_N(A)\right] = \frac{v_+(A)}{2}\,. \tag{21}$$

This proves Eq. (14) for $A \in (A_1^*, A_2^*]$, since in this regime $v_-(A) = 0$.

Finally, for $A \in (A_2^*, \infty)$, it is easy to prove that $\tau_+(A)/\tau_-(A)$ is a continuous strictly increasing function of A which takes values in the interval $(0, 1)$. Let us assume first that for a given $A \in (A_2^*, \infty)$ the ratio $\tau_+(A)/\tau_-(A)$ is a rational number p/q, with $p < q$. Then, if we choose the time period of $F(t)$ as $T = 2Nq\tau_+(A) = 2Np\tau_-(A)$, with $N = 1, 2, 3, \ldots$, the particle travels a distance equal to $N(q-p)$ every time period. Consequently, all the frequencies

$$\omega_N(A) = \frac{\pi}{Nq\tau_+(A)} = \frac{\pi}{Np\tau_-(A)} \tag{22}$$

lead to the same value of the drift velocity

$$v\left[A, \omega_N(A)\right] = \frac{N(q-p)}{2Nq\tau_+(A)} = \frac{1}{2\tau_+(A)} - \frac{1}{2\tau_-(A)} = \frac{v_+(A)+v_-(A)}{2}\,. \tag{23}$$

Taking into account once again that $\lim_{N\to\infty} \omega_N(A) = 0$, it follows that

$$v_{\rm ad}(A) = \lim_{N\to\infty} v\left[A, \omega_N(A)\right] = \frac{v_+(A) + v_-(A)}{2}\,. \tag{24}$$

Since any irrational number can be approximated as closely as desired by a sequence of rational numbers, Eq. (14) is also valid if $\tau_+(A)/\tau_-(A)$ is an irrational number.

In Fig. 6 we present the adiabatic drift velocity in Eq. (14) as a function of the driving amplitude A. We have also plotted the numerical drift velocity obtained for $\omega = 0.01$. Both results are indistinguishable within the resolution of the plot.

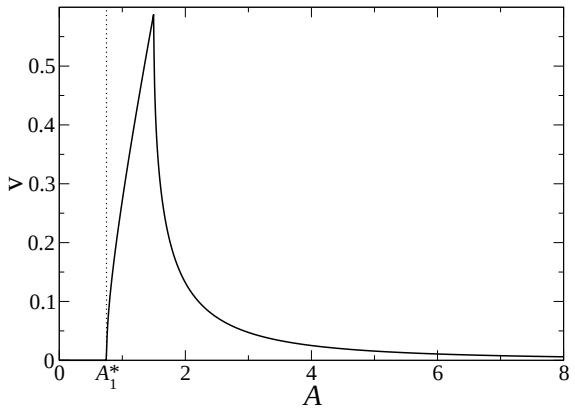

Fig. 6. Drift velocity v (solid line) as a function of the driving amplitude A in the adiabatic limit ($\omega \to 0$). The curve is indistinguishable from the numerical results obtained with $\omega = 0.01$. (All quantities in dimensionless units.)

Finally, from the above argument, another conclusion follows. As mentioned before, the adiabatic value $v_{\rm ad}(A)$ is reached not only in the limit $\omega \to 0$, but also for the finite frequencies given by Eqs. (19) and (22). This result becomes manifest in Figs. 3 and 4, as an infinite number of intersections between the horizontal line (adiabatic limit) and the drift velocity curve. These frequencies are at the core (see the red regions in Fig. 2) of the above discussed fingers. Furthermore, they correspond to exact displacements of n spatial periods for every driving period T. This fact, together with the interpretation provided by our analysis of the zero-current bands, lead us to infer that each finger corresponds to motion in which the particle advances a distance of about n spatial periods at those time intervals when $F(t) = A$. We have checked this fact in the numerical simulations.

4. Conclusions

To summarize, we have studied a one-dimensional deterministic ratchet model in the overdamped regime driven by a rectangular force. We have performed extensive numerical calculations, which allowed us to present a colored phase diagram showing the drift velocity as a function of a wide range

of the driving parameter values A and ω. In addition, we have studied the conditions leading to bounded particle motion, obeying asymptotically periodic, bounded motion, $x(t+T) = x(t)$. We have shown that the resulting regions cover most of the phase space where there is no directed current. Moreover, we have provided an explicit analytical expression for the drift velocity in the adiabatic limit. Finally, the theoretical considerations are of great help to rationalize the finger-shaped structure shown in the diagram.

We (DC, JC-P, AA, MM) acknowledge the support of the Ministerio de Educación y Ciencia of Spain (FIS2005-02884) and the Junta de Andalucía. DC also acknowledges the Ministerio de Educación y Ciencia of Spain for a contract under the Juan de la Cierva program. The authors wish Professor Talkner many more enjoyable years of doing trend-setting science and personal happiness.

REFERENCES

[1] P. Hänggi, R. Bartussek, *Lect. Notes Phys.* **476**, 294 (1996).

[2] R.D. Astumian, P. Hänggi, *Physics Today* **55**, (No. 11), 33 (2002).

[3] H. Linke, *Appl. Phys.* **A75**, 167 (2002).

[4] P. Hänggi, F. Marchesoni, F. Nori, *Ann. Phys. (Leipzig)* **14**, 51 (2005).

[5] P. Reimann, P. Hänggi, *Appl. Phys.* **A75**, 169 (2002).

[6] F. Jülicher, A. Adjari, J. Prost, *Rev. Mod. Phys.* **69**, 1269 (1997).

[7] P. Jung, J.G. Kissner, P. Hänggi, *Phys. Rev. Lett.* **76**, 3436 (1996).

[8] J.L. Mateos, *Phys. Rev. Lett.* **84**, 258 (2000).

[9] S. Sengupta, R. Guantes, S. Miret-Artes, P. Hänggi, *Physica A* **338**, 406 (2004).

[10] F. Family, H.A. Larrondo, D.G. Zarlenga, C.M. Arizmendi, *J. Phys. Cond. Matt.* **17**, S3719 (2005).

[11] R. Bartussek, P. Hänggi, J.G. Kissner, *Europhys. Lett.* **28**, 459 (1994).

[12] A. Sarmiento, H. Larralde, *Phys. Rev.* **E59**, 4878 (1999).

[13] M.N. Popescu, C.M. Arizmendi, A.L. Salas-Brito, F. Family, *Phys. Rev. Lett.* **85**, 3321 (2000).

[14] M. Kostur, P. Hänggi, P. Talkner, J.L. Mateos, *Phys. Rev.* **E72**, 036210 (2005).

[15] A. Adjari, D. Mukamel, L. Peliti, J. Prost, *J. Phys. I (France)* **4**, 1551 (1994).

[16] I. Goychuk, P. Hänggi, *Lect. Notes Phys.* **557**, 7 (2000).

[17] `http://www.netlib.org/ode/rksuite/`.